Analytical modeling of adaptive optics: foundations of the phase spatial power spectrum approach

Laurent Jolissaint and Jean-Pierre Véran

Herzberg Institute of Astrophysics, National Research Council of Canada, 5071 West Saanich Road, Victoria, British Columbia, V9E 2E7, Canada

Rodolphe Conan

Office National d'Etudes et de Recherches Aérospatiales, 29, avenue de la Division Leclerc, F-92322 Châtillon Cedex, France

Received February 11, 2005; accepted May 2, 2005

End-to-end simulation of adaptive optics (AO) systems allows high-fidelity modeling of system performance, but at the cost of long computation time. Analytical modeling, on the other hand, can provide much faster first-order performance estimates for a rapid exploration of the AO parameter space. In this paper, we present the foundations of a modeling method for the AO optical transfer function, based on an analytical description of the residual phase spatial power spectrum. The method has been implemented in an IDL-based code, PAOLA, and comparison with end-to-end simulations demonstrates the validity of the analytical approach.

OCIS codes: 010.1080, 070.2580, 110.4850, 350.1260.

1. INTRODUCTION

Simulation tools are critically important for the development of adaptive optics (AO). They serve a wide range of purposes, including assisting with the design of a new system, debugging an existing system, or predicting the feasibility of a science program on a given system. However, all these applications do not require the same level of accuracy in the results, and therefore the same degree of fidelity in the modeling.

High-fidelity modeling is usually based on numerical methods: The physical properties of each element of the AO system are modeled numerically and can be represented as a block, with one or several inputs/outputs and one or several parameters. For example, the wavefront sensor (WFS) block takes a phase map as input, produces a set of measurements as output and has several parameters, e.g., those specifying the number of subapertures, the pixel size of the detector, etc. Then, the simulation links all the blocks together and executes them sequentially. This approach can potentially model all the optical effects from the source to be observed to the focal plane of the science instrument, and is therefore sometimes called end-to-end (E2E) simulation. Since some blocks are stochastic in nature, for example the simulation of atmospheric turbulence, the whole simulation has to be iterated over many time steps, where new realizations of the stochastic processes are computed for each time step. This is called the Monte Carlo (MC) approach. In order to generate results that are characteristic of the system under study, many iterations have to be completed, and the results for all the iterations analyzed statistically. For example, the end result of one iteration is usually an instantaneous point-spread function (PSF), and by averaging several seconds' worth of instantaneous PSF, one gets an estimate of the long-exposure PSF characteristic of the performance of the AO system. With this type of method, the full statistical description of the PSF is in fact available, including all the statistical moments of the complex electromagnetic field, which can be very useful for specialized applications such as coronagraphy.

It is worth noting in this framework of high-fidelity, E2E MC methods, that the actual level of modeling of each component can vary greatly. For example, the WFS can be modeled using either geometrical optics or diffraction optics, the latter being more accurate, but more computationally intensive. So, several simulation codes exploring different complexity trade-offs have been proposed in the past (see Le Louarn[1] for a review). However, all these codes have in common that, for a given level of modeling, their computational complexity increases greatly with the size of the AO system (i.e., number of actuators). Astronomical AO systems for the current generation of 8 m telescopes typically require from a few hundred to a few thousand actuators. Computing a single long-exposure PSF for such a system using a few seconds worth of AO simulated data can already take several hours on a high-end personal computer. The ongoing studies for the next generation of telescopes (30–100 m) may require days for the computation of a single PSF, which is clearly impractical unless some parallelization schemes are implemented.

Analytical modeling approaches are interesting alter-

natives to numerical modeling. The objective here is to compute directly the long exposure PSF or/and its second-order statistics (see for instance Fusco and Conan[2]) using analytical expressions without requiring any iteration. Only first-order modeling is possible; however, the computational complexity is much reduced. In fact, there are many applications for which high-fidelity modeling is not important, but computation time is critical. This is the case, for example, when doing the initial design of an AO system, where the AO parameter space (number of actuators, number of guide stars, sampling time, etc) has to be explored quickly in order to make the initial trade-offs. More complex modeling through numerical methods can be used afterwards, but only in a few promising cases.

In this paper, we present a method for the analytical modeling of the long-exposure, AO-corrected optical transfer function (OTF) from which the long-exposure, AO-corrected PSF can be obtained via a single numerical Fourier transform. Our approach follows a preliminary derivation from Rigaut *et al.*[3] that we later expanded in two dimensions[4] in order to model the two-dimensional structure of the PSF, not just its one-dimensional average profile. The method is based on the modeling of the residual AO-corrected, phase spatial power spectrum from which, as we will show, a good approximation of the long-exposure OTF can be calculated. In this preliminary work, though, correlation between anisoplanatism and servo-lag AO error was not taken into account, nor was the two-dimensional structure of the WFS aliasing error. These issues are addressed and solved in this paper.

The main objective of this paper is to present the principle of the phase spatial power-spectrum method, its assumptions and limitations. As a support to the demonstration of the method, we develop here the simplest AO system mode: single deformable mirror (DM) with square actuator geometry, single natural guide star (NGS), and a Shack–Hartmann type WFS in an open-loop configuration. This model already includes the five most fundamental limits of any NGS-based AO system: fitting error, WFS aliasing, angular anisoplanatism, servo-lag, and WFS noise. On this theoretical basis, it is possible to develop more sophisticated modeling, including for instance closed-loop AO, laser-guide-star AO, etc. Actually, some of these new developments have already been published [see for instance ground-layer AO (GLAO) spatial power spectrum modeling by Tokovinin[5] and Jolissaint *et al.*[6] and segmented telescope active optics modeling in the spatial frequency domain by Jolissaint and Lavigne[7]], but without discussion of the principle of the power spectrum method. We hope the current paper will provide such a reference analysis. It is worth noting that Ellerbroek[8] very recently published an interesting description of AO modeling in the linear and spatial frequency domain, as we do here, but using a different formulation and a somewhat more sophisticated approach.

In Sections 2 and 3, we show the relationship between the long-exposure OTF and the residual phase spatial power spectrum (PS). In Section 4, we derive the analytical model of the phase PS for the classical AO configuration introduced above. In section 5, we present PAOLA (Performance of Adaptive Optics for Large or Little Apertures), an IDL-based code that implements our method and that has already been used for several studies.[9–14]

2. OPTICAL TRANSFER FUNCTION OF TELESCOPE WITH ADAPTIVE OPTICS

In this section, we explain how the long-exposure OTF of the system "telescope and adaptive optics" (TSC+AO) is calculated from the product of the AO and telescope OTFs. This topic has already been addressed by Conan[15] and Véran,[16] but we revisit it here in the context of our analytical model, including static aberrations.

The instantaneous phase can be written as the sum of a static $\bar{\varphi}$ and a zero-mean, space-time-dependent turbulent term $\delta\varphi$

$$\varphi(\mathbf{r},t) = \bar{\varphi}(\mathbf{r}) + \delta\varphi(\mathbf{r},t). \tag{1}$$

The OTF of an optical system is given by the phasor autocorrelation in the pupil. So it becomes, for the TSC+AO, long-exposure OTF (the time average of the instantaneous OTF),

$$\mathrm{OTF}_{\mathrm{sys}}(\mathbf{f}) = \frac{1}{S_p}\int\int_{\mathbb{R}^2} \langle \exp\{i[\delta\varphi(\mathbf{r},t) - \delta\varphi(\mathbf{r}+\boldsymbol{\rho},t)]\}\rangle_t \times \exp\{i[\bar{\varphi}(\mathbf{r}) - \bar{\varphi}(\mathbf{r}+\boldsymbol{\rho})]\} P(\mathbf{r})P(\mathbf{r}+\boldsymbol{\rho})\mathrm{d}^2 r, \tag{2}$$

where the frequency in the focal plane is associated with a position in the pupil plane through $\mathbf{f}=\boldsymbol{\rho}/\lambda$, λ being the optical wavelength. $P(\mathbf{r})$ is the pupil transmission mask (1 in the pupil, 0 outside) and S_p the pupil area. We assume here that the amplitude fluctuations of the electromagnetic field are negligible within the pupil, as if the phase-turbulent perturbation were occurring so close to the pupil that the amplitude change due to Fresnel propagation can be neglected. This so-called "near-field approximation" is very common in AO, and can be proved to be satisfactory in most cases.[17] With the assumption that the time-variable component of the phase $\delta\varphi$ has Gaussian statistics, which is a good assumption even in the case of an AO-corrected residual phase, it can be shown[17] that the time average can be moved into the exponential, to get

$$\mathrm{OTF}_{\mathrm{sys}}(\mathbf{f}) = \frac{1}{S_p}\int\int_{\mathbb{R}^2} \exp[-1/2\langle F_\varphi^2(\mathbf{r},\boldsymbol{\rho},t)\rangle_t] \times \exp\{i[\bar{\varphi}(\mathbf{r}) - \bar{\varphi}(\mathbf{r}+\boldsymbol{\rho})]\} P(\mathbf{r})P(\mathbf{r}+\boldsymbol{\rho})\mathrm{d}^2 r, \tag{3}$$

where $F_\varphi(\mathbf{r},\boldsymbol{\rho},t) \equiv \varphi(\mathbf{r},t) - \varphi(\mathbf{r}+\boldsymbol{\rho},t)$ defines the statistical increment of the turbulent phase.[18]

A. Turbulent Phase Optical Transfer Function

Locally, the turbulent phase (no AO correction) can be considered stationary. So, the increment will depend only on the distance $\boldsymbol{\rho}$ between two points, and not on the absolute location $\mathbf{r}$ of these points: $F_\varphi(\mathbf{r},\boldsymbol{\rho},t) = F_\varphi(\boldsymbol{\rho},t)$. In this case, we can define a variance for the statistical increment, which is commonly called the structure function,

$$D_\varphi(\boldsymbol{\rho}) \equiv \langle F_\varphi^2(\boldsymbol{\rho},t)\rangle_t, \tag{4}$$

here the phase structure function. As the turbulent phase is isotropic, only the modulus of $\boldsymbol{\rho}$ is of importance, and it can be shown[17] that

$$D_\varphi(\rho) = 6.883877(\rho/r_0)^{5/3}, \tag{5}$$

where r_0 is the Fried parameter,[19] a measure of the coherent scale of the turbulent phase at the given wavelength. As a consequence, the exponential of the structure function can be removed from the integral, Eq. (3), and we obtain

$$\begin{aligned}\mathrm{OTF}_{\mathrm{sys}}(\mathbf{f}) &= \exp[-D_\varphi(\lambda f)/2]\frac{1}{S_p}\int\int_{\mathbb{R}^2}\exp\{i[\bar{\varphi}(\mathbf{r}) \\ &\quad - \bar{\varphi}(\mathbf{r}+\lambda\mathbf{f})]\}P(\mathbf{r})P(\mathbf{r}+\lambda\mathbf{f})\mathrm{d}^2r \\ &= \mathrm{OTF}_{\mathrm{atm}}(|\mathbf{f}|)\mathrm{OTF}_{\mathrm{tsc}}(\mathbf{f}),\end{aligned} \tag{6}$$

so that the final OTF is given as a product of two components: The first one carries the second-order statistic of the zero-mean turbulent phase, and defines the turbulent atmosphere $\mathrm{OTF}_{\mathrm{atm}}$; the second one, the static $\mathrm{OTF}_{\mathrm{tsc}}$, carries the contribution of the telescope (diffraction limit and static aberrations) and the science instrument (CCD OTF, for instance). The fact that the OTF can be split this way makes it very simple to compute the long-exposure PSF for a given telescope.

B. Adaptive-Optics-Corrected Phase Optical Transfer Function

In the AO-corrected case, the phase is not stationary in the pupil,[15] so the location dependence $\mathbf{r}$ in the increment and in the AO-corrected structure function remains $D_\varphi^{\mathrm{ao}}(\mathbf{r},\boldsymbol{\rho}) = \langle F(\mathbf{r},\boldsymbol{\rho},t)\rangle$. A $\boldsymbol{\rho}$-dependent-only structure function cannot be defined. So, if we want to split the global OTF between an AO and a telescope component, we have no choice but to assume that the phase *is* corrected homogeneously everywhere in the $\mathbb{R}^2$ plane, as if the DM were infinitely large. In that approximation, the corrected phase is stationary, and it is possible to define a structure function that is a function only of the separation vector between points in the telescope pupil. Unlike the noncorrected case, though, this stationary structure function, which we will write $D_\varphi^\infty(\boldsymbol{\rho})$ [$\mathbf{r}$ average of $D_\varphi^{\mathrm{ao}}(\mathbf{r},\boldsymbol{\rho})$ within the pupil], is not necessarily isotropic: One can consider for instance the case of an off-axis correction, better in the direction of the NGS than in the perpendicular direction. Removing the structure-function exponential from the integral Eq. (3), we can now write the system's OTF as

$$\begin{aligned}\mathrm{OTF}_{\mathrm{sys}}(\mathbf{f}) &\approx \exp[-D_\varphi^\infty(\lambda\mathbf{f})/2]\frac{1}{S_p}\int\int_{\mathbb{R}^2}\exp\{i[\bar{\varphi}(\mathbf{r}) \\ &\quad - \bar{\varphi}(\mathbf{r}+\lambda\mathbf{f})]\}P(\mathbf{r})P(\mathbf{r}+\lambda\mathbf{f})\mathrm{d}^2r \\ &= \mathrm{OTF}_{\mathrm{ado}}(\mathbf{f})\mathrm{OTF}_{\mathrm{tsc}}(\mathbf{f}).\end{aligned} \tag{7}$$

What is the effect of this stationarity assumption? Equation (7) implies that we approximate the average of the exponential of $D_\varphi^{\mathrm{ao}}(\mathbf{r},\boldsymbol{\rho})$ by the exponential of the average $D_\varphi^\infty(\boldsymbol{\rho})$. Using Jensen's inequality[20]—which states that for a convex function f (as the exponential is), the function of the average of an interval $[a,b]$ is always smaller than the average of the function in this interval, i.e., $f(\langle[a,b]\rangle) \leqslant \langle[f(a),f(b)]\rangle$—we find that the total OTF given in Eq. (7) underestimates the real OTF. Using numerical simulation, Véran[21] basically found the same result. He found also that the OTF error increases with the focal plane angular frequency and with D/r_0 but decreases with the order of correction, and that the absolute error, in the worst case, is of the order of 0.02 on the Strehl ratio. So, we think it is reasonable, keeping in mind the objective of our model, to accept this approximation.

3. RELATIONSHIP BETWEEN PHASE STRUCTURE FUNCTION AND PHASE POWER SPECTRUM

In developing Eq. (4), it happens that the phase structure function is related to the phase autocorrelation[18] B_φ, $D_\varphi(\boldsymbol{\rho}) = 2[B_\varphi(0) - B_\varphi(\boldsymbol{\rho})]$. Now, as the phase autocorrelation is the Fourier transform (FT) of the phase PS, it is easy to show that

$$D_\varphi(\boldsymbol{\rho}) = 2\int\int_{\mathbb{R}^2}[1-\cos(2\pi\mathbf{f}\cdot\boldsymbol{\rho})]\Xi\{\delta\varphi\}(\mathbf{f})\mathrm{d}^2f, \tag{8}$$

where $\Xi\{\delta\varphi\}$ denotes the phase spatial PS. This equality is of general use, and applies either to the turbulent phase or the AO-corrected phase (assuming stationarity).

The AO structure function can be computed by numerical integration of Eq. (8) [via fast Fourier transform (FFT)] once an analytical expression for the phase PS is known. Then the system total OTF can be computed using Eq. (6) or Eq. (7). The central point of the analytical approach is then the calculation of the residual phase spatial PS, $\Xi\{\delta\varphi\}$. We develop this in Section 4.

4. ADAPTIVE OPTICS RESIDUAL PHASE POWER SPECTRUM

In this section, we develop the calculation of the residual phase PS in two dimensions, following the same procedure as Rigaut *et al.*[3] did for the one-dimensional case. Note that only the zero-average, residual turbulent phase $\delta\varphi$ is of interest here; the static phase is taken into account in the telescope OTF.

A. Principle of the Power Spectrum Method

The fundamental equation of AO is our starting point:

$$\delta\varphi_r(\mathbf{r},\boldsymbol{\theta},t) = \delta\varphi_a(\mathbf{r},\boldsymbol{\theta},t) - \widetilde{\delta\varphi_a}(\mathbf{r},0,t), \tag{9}$$

meaning that the residual of the corrected phase $\delta\varphi_r$ is given, when looking in a field direction angle $\boldsymbol{\theta}$, by the difference between the atmospheric turbulent phase $\delta\varphi_a$ seen in that direction and the on-axis turbulent phase estimated from the on-axis NGS, $\delta\widetilde{\varphi}_a$. The fundamental limits of AO systems make this residual phase nonzero, and five components can be identified: First, the WFS has a finite spatial sampling, set by the subaperture size Δ_{WFS} as seen from the pupil plane, so spatial frequencies above the WFS Nyquist frequency $f_{\mathrm{WFS}} = (2\Delta_{\mathrm{WFS}})^{-1}$ are not sensed, and cannot be corrected. Now, even if the WFS

does not have such a limitation, the DM will be able to correct only the phase fluctuations below its cutoff frequency $f_{\mathrm{DM}}=(2\Delta_{\mathrm{DM}})^{-1}$, where Δ_{DM} is the actuator pitch, as seen from the pupil plane. As a consequence, the highest spatial frequency the AO system will be able to correct is defined by the minimum of both WFS and DM cutoff frequencies. In most systems, though, the subaperture size matches the DM actuator pitch, and we have $\Delta_{\mathrm{WFS}}=\Delta_{\mathrm{DM}} \equiv \Lambda$. Here, we will assume this is the case, and will define the cutoff frequency of the AO system with $f_{\mathrm{AO}}=(2\Lambda)^{-1}$. Also, we will assume that the filtering is a perfect high-pass: complete filtering below f_{AO}, and complete transmission above. These uncorrected high spatial frequencies are transmitted to the output of the AO system, and make for the first and larger error term, frequently referred to as the fitting error. Second, the non-sensed high spatial frequencies (above f_{AO}) are aliased in the low-frequency domain of the WFS, making for the second most important source of error, the phase aliasing error. Third, to get a good signal-to-noise ratio (SNR) on the phase measurement, the WFS has to sense for a certain integration time Δt, which is a trade-off between getting enough NGS photons and not averaging too much the phase high-temporal fluctuations. In other words, the integration time is chosen to minimize the added contributions of the WFS noise and time averaging. Moreover, the reading of the WFS CCD, the phase reconstruction, and the DM's surface update takes some time (roughly one sampling period), creating a time lag between phase measurement and correction. The phase error term associated with both time averaging and time lag is called the servo-lag error. The fourth error term is naturally due to the WFS noise, and is called the noise error. Finally, as turbulence is highly anisoplanatic (the isoplanatic patch is of the order of a few arc seconds in the visible wavelengths), there will be an isoplanatic error for off-axis science targets. Of course, there might be other unexpected sources of residual phase errors (vibrations, for instance) but these are not due to the fundamental limits of AO systems, and can be avoided, in principle, by a proper design of the system. We will then not consider these potential sources of error in this paper, even though it is certainly possible to model some of them analytically.

The time sequence of the AO loop is split in a WFS integration time Δt, immediately followed by a delay ξ due to WFS reading and phase reconstruction. So the phase is corrected at a time $\Delta t+\xi$ after the beginning of the WFS measure. As the ideal scheme would be to apply the correction in the middle of the integration time, the total servo lag is $t_l=\Delta t/2+\xi$.

Let us write $\mathcal{M}$ as the measurement operator in the pupil plane. Its exact formulation depends on the WFS type, but for now we can keep a general notation. The measure $m(\mathbf{r},t)$ is the application of $\mathcal{M}$ on the phase averaged over the integration time, plus the WFS noise $\nu(\mathbf{r},t)$:

$$m(\mathbf{r},t) = \mathcal{M}\left\{\frac{1}{\Delta t}\int_{-\Delta t/2}^{\Delta t/2} \delta\varphi_a(\mathbf{r},0,t'+t-t_l)\mathrm{d}t'\right\} + \nu(\mathbf{r},t) = \mathcal{M}\{\overline{\delta\varphi_a}(\mathbf{r},0,t)\} + \nu\{\mathbf{r},t\}, \tag{10}$$

where the overline represents the average over the WFS integration time Δt of the time-lagged phase. Note that this finite time average should not be confused with the exposure time average, which is defined here for the full AO exposure time, assumed infinite. Finally, the WFS measure is sent to the reconstructor $\mathcal{R}$ to get an estimation of the on-axis turbulent phase (recall that we assume an on-axis NGS and an off-axis science target):

$$\widetilde{\delta\varphi_a}(\mathbf{r},0,t) = \mathcal{R}\{\mathcal{M}[\overline{\delta\varphi_a}(\mathbf{r},0,t)]\} + \mathcal{R}\{\nu(\mathbf{r},t)\}. \tag{11}$$

Now the phase, whatever its origin, can be written as a Fourier decomposition, where the coefficients are given by the phase FT, $\hat{\delta\varphi}(\mathbf{f},t)$, and the basis functions by the infinite set of complex exponentials, $\exp[2\pi i(xf_x+yf_y)]$:

$$\delta\varphi(\mathbf{r},t) = \int\int_{\mathbb{R}^2} \hat{\delta\varphi}(\mathbf{f},t)\exp[2\pi i(xf_x+yf_y)]\mathrm{d}^2 f. \tag{12}$$

The space vector defined by the set of the complex exponentials can be split into two subspaces: a low-frequency (LF) one associated with the spatial frequencies the AO system can correct, below f_{AO}, and a high-frequency (HF) one associated with the spatial frequencies the system cannot correct, above f_{AO}.

Let us decompose the phase into its projection onto these two subspaces: $\delta\varphi_{\mathrm{LF}}$ defines the LF component, $\delta\varphi_{\mathrm{HF}}$ the HF one:

$$\delta\varphi = \delta\varphi_{\mathrm{LF}} + \delta\varphi_{\mathrm{HF}}. \tag{13}$$

Splitting the atmospheric phase into its two components according to Eq. (13), and inserting it into the fundamental equation of AO, Eq. (9), it becomes, with Eq. (11)

$$\delta\varphi_r(\mathbf{r},\boldsymbol{\theta},t) = \delta\varphi_{\mathrm{LF},a}(\mathbf{r},\boldsymbol{\theta},t) + \delta\varphi_{\mathrm{HF},a}(\mathbf{r},\boldsymbol{\theta},t) - \mathcal{R}\{\mathcal{M}[\overline{(\delta\varphi_{\mathrm{LF},a}+\delta\varphi_{\mathrm{HF},a})}(\mathbf{r},0,t)]\} - \mathcal{R}\{\nu(\mathbf{r},t)\}. \tag{14}$$

Here comes another model assumption: The reconstructor is able to reconstruct perfectly the LF term of the phase from its measurement $m_{\mathrm{LF}}=\mathcal{M}\{\delta\varphi_{\mathrm{LF}}\}$, allowing us to write

$$\mathcal{R}(m_{\mathrm{LF}}) = \mathcal{R}\{\mathcal{M}[\delta\varphi_{\mathrm{LF}}]\} = \delta\varphi_{\mathrm{LF}}. \tag{15}$$

The application of the measurement operator $\mathcal{M}$ on both $\delta\varphi_{\mathrm{LF}}$ and the noise is separated, and the aliasing term involves only the HF term $\delta\varphi_{\mathrm{HF}}$. This assumption is then quite reasonable. By use of Eq. (15), Eq. (14) can now be written as the sum of five terms (the five errors introduced above):

$$\delta\varphi_r(\mathbf{r},\boldsymbol{\theta},t) = \underbrace{\delta\varphi_{\mathrm{HF},a}(\mathbf{r},\boldsymbol{\theta},t)}_{\delta\varphi_{\mathrm{HF},a}} + \underbrace{\delta\varphi_{\mathrm{LF},a}(\mathbf{r},\boldsymbol{\theta},t) - \delta\varphi_{\mathrm{LF},a}(\mathbf{r},0,t)}_{\delta\varphi_{\mathrm{LF},\theta}} + \underbrace{\delta\varphi_{\mathrm{LF},a}(\mathbf{r},0,t) - \overline{\delta\varphi_{\mathrm{LF},a}}(\mathbf{r},0,t)}_{\delta\varphi_{\mathrm{LF},s}} - \underbrace{\overline{\mathcal{R}\{\mathcal{M}[\delta\varphi_{\mathrm{HF},a}]\}}(\mathbf{r},0,t)}_{\delta\varphi_{\mathrm{LF,HF}}} - \underbrace{\mathcal{R}\{\nu(\mathbf{r},t)\}}_{\delta\varphi_{\mathrm{LF},n}} \tag{16}$$

where we have subtracted and added the on-axis LF phase to make the anisoplanatism and the servo-lag terms appear individually. The first term on the right-hand side of Eq. (16) is the fitting error $\delta\varphi_{\mathrm{HF},a}$ (high fre-

quency); the second term is the phase anisoplanatism $\delta\varphi_{\mathrm{LF},\theta}$; the third term is the phase servo lag $\delta\varphi_{\mathrm{LF},s}$; the fourth term is the phase aliasing $\delta\varphi_{\mathrm{LF,HF}}$, and the last term is the phase noise $\delta\varphi_{\mathrm{LF},n}$. The latter four terms are low-frequency ones.

Let us now develop the residual phase PS. It is defined by the modulus square of the residual phase FT, averaged over the (infinite) exposure time:

$$\begin{aligned}\Xi(\delta\varphi_r)(\mathbf{f}) = \langle|\hat{\delta\varphi}_r(\mathbf{f},\boldsymbol{\theta},t)|^2\rangle &= \langle|\hat{\delta\varphi}_{\mathrm{HF},a}(\mathbf{f},\boldsymbol{\theta},t)|^2\rangle \\ &+ \langle|\hat{\delta\varphi}_{\mathrm{LF},\theta}(\mathbf{f},\boldsymbol{\theta},t)|^2\rangle + \langle|\hat{\delta\varphi}_{\mathrm{LF},s}(\mathbf{f},0,t)|^2\rangle \\ &+ \langle|\hat{\delta\varphi}_{\mathrm{LF,HF}}(\mathbf{f},0,t)|^2\rangle + \langle|\hat{\delta\varphi}_{\mathrm{LF},n}(\mathbf{f},t)|^2\rangle + \mathrm{CS}.\end{aligned} \tag{17}$$

Let us analyze the cross-spectrum (CS) terms. First, we note that among the ten possible CS terms, those including the noise term vanish, because the noise is in principle not correlated with the other phase terms. Second, as we have split the spatial frequency space into two distinct LF and HF domains, products between LF and HF spectra do not overlap, so they automatically vanish. So do the associated CS terms. Finally, only the correlation between anisoplanatism and servo lag is left:

$$\begin{aligned}\mathrm{CS} = &\langle\widehat{\delta\varphi}_{\mathrm{LF},\theta}(\mathbf{f},\boldsymbol{\theta},t)\,\widehat{\delta\varphi}^{*}_{\mathrm{LF},s}(\mathbf{f},0,t)\rangle \\ &+ \langle\widehat{\delta\varphi}^{*}_{\mathrm{LF},\theta}(\mathbf{f},\boldsymbol{\theta},t)\,\widehat{\delta\varphi}_{\mathrm{LF},s}(\mathbf{f},0,t)\rangle,\end{aligned} \tag{18}$$

where $*$ denotes complex conjugation. In the following subsections, we derive the expressions for the individual PS of each of the five error terms, plus the aniso–servo CS.

B. Power Spectrum Models of the Piston-Filtered Turbulent Phase

We recall here the expressions for the most commonly used turbulent phase PS: the Kolmogorov model, which holds for an infinite extension of the turbulence at every scale from zero to the infinite,

$${}^{K}\Xi\{\delta\varphi_a\}(f) = 0.0229 r_0^{-5/3} f^{-11/3}, \tag{19}$$

and the Hill–Andrew model (an improvement of the Von Karman model), which takes into account the effect of both the outer and inner scales (L_0, l_0) of turbulence:[22]

$$\begin{aligned}{}^{\mathrm{HA}}\Xi\{\delta\varphi_a\}(f) = &\,0.0229 r_0^{-5/3}(f^2 + 1/L_0^2)^{-11/6} \\ &\times[1 + 3.43 f l_0 + 0.538(f l_0)^{7/6}] \\ &\times\exp(-3.625 f^2 l_0^2).\end{aligned} \tag{20}$$

The PS for individual layers can be written by replacing the global Fried parameter r_0 by the layer's value. Note that the phase average over the entrance pupil of the telescope (the piston mode) cannot be seen by the AO system, and does not participate in image formation. Consequently, such a mode must be filtered out by simple multiplication of the turbulent phase PS with the piston filter[23]

$$F_p(f) = 1 - \left[\frac{2J_1(\pi D f)}{\pi D f}\right]^2, \tag{21}$$

where D is the telescope pupil diameter.

C. Fitting-Error Power Spectrum

According to our assumption, the AO system is able to correct perfectly the phase aberrations at every spatial frequency below f_{AO}, and reflects the HF phase to the output of the system. The PS of the HF phase (fitting error) is then simply the truncated, piston-filtered, turbulent phase PS (any model M) set to zero in the low-spatial-frequency domain:

$$\Xi\{\delta\varphi_{\mathrm{HF},a}\}(\mathbf{f}) = \mu_{\mathrm{HF}}(\mathbf{f})F_p(f)\,{}^{\mathrm{M}}\Xi\{\delta\varphi_a\}(f), \tag{22}$$

where the mask μ_{HF} is 1 for frequencies above f_{AO} and 0 elsewhere. For the particular case of a Shack–Hartmann and DM with square lenslets/actuators geometry, the LF domain is defined by $|f_x|, |f_y| < f_{\mathrm{AO}}$ (a square); other WFS geometry will give other LF domain boundaries (for instance, a disk for a curvature-sensing WFS). Here, a square geometry will be considered.

D. Anisoplanatism Power Spectrum

Let us define $\delta\varphi_a[h]$ as the phase aberration due to a turbulent layer at an altitude h relative to the entrance pupil. As seen from the pupil plane, at an angle $\boldsymbol{\theta}$ from the optical axis (science object position in the field), this phase aberration becomes $\delta\varphi_a(\mathbf{r},\boldsymbol{\theta},t) = \delta\varphi_a[h](\mathbf{r} + h\boldsymbol{\theta}, t)$. If there are N turbulent layers, the total atmospheric phase aberration becomes

$$\delta\varphi_a(\mathbf{r},\boldsymbol{\theta},t) = \sum_{n=1}^{N} \delta\varphi_a[h_n](\mathbf{r} + h_n\boldsymbol{\theta}, t). \tag{23}$$

Now, we can compute the FT of the phase anisoplanatism $\delta\varphi_{\mathrm{LF},\theta}$. With Eq. (23), and using the shift theorem of the FT, it becomes:

$$\widehat{\delta\varphi}_{\mathrm{LF},\theta}(\mathbf{f},\boldsymbol{\theta},t) = \sum_{n=1}^{N} \widehat{\delta\varphi}_{\mathrm{LF},a}[h_n](\mathbf{f},t)[\exp(2\pi i h_n \mathbf{f}\cdot\boldsymbol{\theta}) - 1], \tag{24}$$

from which we can get the angular anisoplanatism PS (using the assumption that the turbulent layers are independent):

$$\begin{aligned}\Xi\{\delta\varphi_{\mathrm{LF},\theta}\}(\mathbf{f},\boldsymbol{\theta}) = &\,2\mu_{\mathrm{LF}}(\mathbf{f})F_p(f)\sum_{n=1}^{N} {}^{\mathrm{M}}\Xi\{\delta\varphi_a[h_n]\}(f) \\ &\times[1 - \cos(2\pi h_n \mathbf{f}\cdot\boldsymbol{\theta})],\end{aligned} \tag{25}$$

where the mask $\mu_{\mathrm{LF}} = 1 - \mu_{\mathrm{HF}}$ is 1 for $|f_x|, |f_y| < f_{\mathrm{AO}}$ and 0 elsewhere, and where ${}^{\mathrm{M}}\Xi\{\delta\varphi_a[h_n]\}$ is the turbulent-phase PS of layer n (Subsection 4.B).

E. Servo-Lag Power Spectrum

We compute now the PS of the phase servo lag $\delta\varphi_{\mathrm{LF},s}$. Let us assume that the time scale of the turbulent flow dynamical evolution is much longer than the total time lag of our AO system. With the assumption that the turbulence is stratified in N independent horizontal layers, the

phase at each layer output can be seen as a frozen screen propagated horizontally at constant velocity and direction across the telescope beam—the so-called Taylor hypothesis. Projected in the pupil plane, a τ time-shifted phase at altitude h can be seen as the same phase spatially shifted in the direction backward to the wind, $-\mathbf{v}$, by the distance crossed during the time τ: $\delta\varphi_a[h](\mathbf{r},t+\tau) = \delta\varphi_a[h](\mathbf{r}-\mathbf{v}[h]\tau,t)$. For N layers, the total phase aberration in the pupil plane becomes

$$\delta\varphi_a(\mathbf{r},t+\tau) = \sum_{n=1}^{N} \delta\varphi_a[h_n](\mathbf{r}-\mathbf{v}[h_n]\tau,t). \tag{26}$$

Now, we can compute the FT of $\delta\varphi_{\mathrm{LF},s}$. From its definition in Eq. (16), it becomes

$$\widehat{\delta\varphi}_{\mathrm{LF},s}(\mathbf{f},t) = \widehat{\delta\varphi}_{\mathrm{LF},a}(\mathbf{f},t) - \mathcal{F}\{\overline{\delta\varphi_{\mathrm{LF},a}}(\mathbf{r},t)\}. \tag{27}$$

Let us develop the time-lag-shifted term of Eq. (27). We first replace the time-lagged-shifted phase $\overline{\delta\varphi}$ by its definition in Eq. (10). Then, by use of Eq. (26) and the shift theorem of the FT, it becomes:

$$\mathcal{F}\{\overline{\delta\varphi_{\mathrm{LF},a}}(\mathbf{r},t)\} = \sum_{n=1}^{N} \widehat{\delta\varphi}_{\mathrm{LF},a}[h_n](\mathbf{f},t) \int_{-\Delta t/2}^{\Delta t/2} \times \exp[-2\pi i(t'-t_l)\mathbf{f}\cdot\mathbf{v}(h_n)]\mathrm{d}t'. \tag{28}$$

Realizing that the integral over $\pm\Delta t/2$ is in fact a time-domain FT of the door function $\Pi(t'/\Delta t)$, we find

$$\mathcal{F}\{\overline{\delta\varphi_{\mathrm{LF},a}}(\mathbf{r},t)\} = \sum_{n=1}^{N} \widehat{\delta\varphi}_{\mathrm{LF},a}[h_n](\mathbf{f},t) \times \mathrm{sinc}[\Delta t\mathbf{f}\cdot\mathbf{v}(h_n)]\exp[2\pi i t_l\mathbf{f}\cdot\mathbf{v}(h_n)]. \tag{29}$$

Finally, substituting Eq. (29) into Eq. (27), and using $\widehat{\delta\varphi}_{\mathrm{LF},a}(\mathbf{f},t) = \Sigma_n \widehat{\delta\varphi}_{\mathrm{LF},a}[h_n](\mathbf{f},t)$, we find

$$\widehat{\delta\varphi}_{\mathrm{LF},s}(\mathbf{f},t) = \sum_{n=1}^{N} \widehat{\delta\varphi}_{\mathrm{LF},a}[h_n](\mathbf{f},t) \times \{1 - \mathrm{sinc}[\Delta t\mathbf{f}\cdot\mathbf{v}(h_n)]\exp[2\pi i t_l\mathbf{f}\cdot\mathbf{v}(h_n)]\}, \tag{30}$$

from which it is easy to compute the servo-lag PS:

$$\Xi\{\delta\varphi_{\mathrm{LF},s}\}(\mathbf{f}) = \mu_{\mathrm{LF}}(\mathbf{f})F_p(f)\sum_{n=1}^{N} {}^{\mathrm{M}}\Xi\{\delta\varphi_a[h_n]\}(f) \times \{1 - 2\cos[2\pi t_l\mathbf{f}\cdot\mathbf{v}(h_n)] \times \mathrm{sinc}[\Delta t\mathbf{f}\cdot\mathbf{v}(h_n)] + \mathrm{sinc}^2[\Delta t\mathbf{f}\cdot\mathbf{v}(h_n)]\}. \tag{31}$$

F. Total Aniso–Servo Power Spectrum

As we have seen above, anisoplanatism and servo-lag errors are not independent, and their cross spectrum must be taken into account. We will not give here the expression for this CS. It is instead much easier to compute the total PS of the combination of both effects, $\Xi\{\delta\varphi_{\theta,s}\} = \Xi\{\delta\varphi_{\mathrm{LF},\theta}\} + \Xi\{\delta\varphi_{\mathrm{LF},s}\} + \mathrm{CS}$, starting from Eq. (16), but without the subtraction/addition of the on-axis LF phase. We have

$$\Xi\{\delta\varphi_{\theta,s}\}(\mathbf{f}) = \langle|\widehat{\delta\varphi}_{\mathrm{LF},a}(\mathbf{f},\boldsymbol{\theta},t)|^2\rangle + \langle|\widehat{\delta\varphi}_{\mathrm{LF},a}(\mathbf{f},0,t)|^2\rangle - 2\,\mathrm{Re}\{\langle\widehat{\delta\varphi}_{\mathrm{LF},a}(\mathbf{f},\boldsymbol{\theta},t)\widehat{\delta\varphi}^{*}_{\mathrm{LF},a}(\mathbf{f},0,t)\rangle\}. \tag{32}$$

Using Eq. (29), calculating the Fourier transform of Eq. (23), and assuming that the turbulent layers are independent, we find

$$\Xi\{\delta\varphi_{\theta,s}\}(\mathbf{f}) = \mu_{\mathrm{LF}}(\mathbf{f})F_p(f)\sum_{n=1}^{N} {}^{\mathrm{M}}\Xi\{\delta\varphi_a[h_n]\}(f) \times (1 - 2\cos\{2\pi\mathbf{f}\cdot[h_n\boldsymbol{\theta} - t_l\mathbf{v}(h_n)]\} \times \mathrm{sinc}[\Delta t\mathbf{f}\cdot\mathbf{v}(h_n)] + \mathrm{sinc}^2[\Delta t\mathbf{f}\cdot\mathbf{v}(h_n)]). \tag{33}$$

It is easy to see that Eq. (33) transforms into Eq. (25) when the integration time is null (no servo lag), and into Eq. (31) when the science target is on-axis (no anisoplanatism).

G. Shack–Hartman Wavefront-Sensor-Measurement Operator $\mathcal{M}$

To compute the other terms of the phase PS (aliasing and noise), we need an explicit expression for the measurement operator $\mathcal{M}$, whose structure depends on the type of WFS. Here, we restrict the discussion to the Shack–Hartman-wavefront-sensor (SH-WFS) case. Other types of WFS can be chosen, though, using the same spatial frequency approach to derive a measurement operator (see for instance Verinaud[24] for the pyramid WFS case).

The SH-WFS-measurement operator is a two-component, two-dimension discrete distribution that implements the derivative of the phase in both x and y directions, averaged over the lenslets area. Let us consider the x component of the measurement. It may be written as

$$m_x(\mathbf{r}) = \mathcal{M}\{\delta\varphi(\mathbf{r},t)\}_x = \left\{\frac{\partial\delta\varphi}{\partial x}(\mathbf{r},t) * \frac{1}{\Lambda^2}[\Pi(x/\Lambda)\Pi(y/\Lambda)]\right\}\mathrm{III}(\mathbf{r}/\Lambda). \tag{34}$$

The convolution with the "door-functions" product expresses the averaging of the phase on square lenslets of width Λ, and the product with the comb function III expresses the spatial sampling of the phase on a Λ-pitch square grid. In principle, we would multiply on the right by the pupil transmission function $P(\mathbf{r})$, but as we are assuming here that the phase is homogeneously corrected everywhere in the (x,y) plane associated with the pupil plane, it is equivalent to assume that the telescope diameter is infinite, so this term is unnecessary. Now, let us compute the FT of Eq. (34). We find

$$\hat{m}_x(\mathbf{f},t) = \Lambda^2 2\pi i[f_x\widehat{\delta\varphi}(\mathbf{f},t)\mathrm{sinc}(\Lambda f_x)\mathrm{sinc}(\Lambda f_y)] * \mathrm{III}(\Lambda\mathbf{f}), \tag{35}$$

where the convolution with the comb function expresses the repetition of the term in brackets in a regularly

$1/\Lambda$-spaced grid in the spatial frequency domain, and is responsible for the aliasing of the HF phase component into the LF domain $|f_x|,|f_y|<f_{\mathrm{AO}}$ (which always occurs, as the turbulent-phase PS is not bounded toward the high spatial frequencies). In the spatial frequency space, the measure is then equivalent to the application—on the instantaneous phase-amplitude spectrum—of the two-component operator

$$\hat{\mathcal{M}} \equiv \Lambda^2 2\pi i[\mathbf{f}\,\mathrm{sinc}(\Lambda f_x)\mathrm{sinc}(\Lambda f_y)] * \mathrm{III}(\Lambda \mathbf{f}). \tag{36}$$

H. Shack–Hartman Wavefront-Sensor-Reconstruction Operator $\mathcal{R}$

Now, we need an expression for the phase-reconstruction operator, or reconstructor, in particular its FT, $\hat{\mathcal{R}}$. Basically, it must be equivalent to the inverse of the measurement-operator FT, $\hat{\mathcal{M}}$, without the aliasing part (as the reconstructed phase is by definition in the LF space), and its exact formulation will depend on the reconstruction algorithm. Here, we will assume a least-square-estimate (LSE) algorithm. It will still be possible to implement other algorithms, as long as practical analytical expressions are available, following the same procedure as presented here. Note also that in our open-loop approach, temporal transfer functions are assumed to be 1, and limited to the temporal frequency range $<1/(2\Delta t)$.

The LSE-reconstructed phase $\widetilde{\delta\varphi_a}$ is determined by the minimization of the quadratic distance ϵ^2 between its own measurement $\mathcal{M}\{\widetilde{\delta\varphi_a}\}$—but without WFS aliasing—and the actual phase measurement $\mathbf{m}(\mathbf{r},t)=[m_x(\mathbf{r},t);m_y(\mathbf{r},t)]$, subject to aliasing, WFS noise, and servo-lag error:

$$\epsilon^2 = \{m_x(\mathbf{r},t) - \mathcal{M}[\widetilde{\delta\varphi_a}(\mathbf{r},0,t)]_x\}^2 + \{m_y(\mathbf{r},t) - \mathcal{M}[\widetilde{\delta\varphi_a}(\mathbf{r},0,t)]_y\}^2. \tag{37}$$

Of course, this minimization can also be done in the Fourier space, and in that case we get the reconstructed phase FT $\widehat{\widetilde{\delta\varphi_a}}$ instead: Replacing Eq. (37) by its FT counterpart, and using Eq. (36) but without the III function, we find, after differentiating $\hat{\epsilon}^2$ relative to $\widehat{\widetilde{\delta\varphi_a}}$ and setting the result equal to zero,

$$\widehat{\widetilde{\delta\varphi_a}}(\mathbf{f},t) = \frac{\hat{m}_x(\mathbf{f},t)f_x + \hat{m}_y(\mathbf{f},t)f_y}{2\pi i f^2\,\mathrm{sinc}(\Lambda f_x)\mathrm{sinc}(\Lambda f_y)} = \hat{\mathcal{R}}\cdot[\hat{m}_x(\mathbf{r},t);\hat{m}_y(\mathbf{r},t)], \tag{38}$$

which can be written as a dot product between the measurement vector $\hat{\mathbf{m}}(\mathbf{f},t)$ and a two-component function representing the reconstructor in the spatial frequency domain,

$$\hat{\mathcal{R}} \equiv \mathbf{f}/[2\pi i f^2\,\mathrm{sinc}(\Lambda f_x)\mathrm{sinc}(\Lambda f_y)]. \tag{39}$$

Now, we have everything we need to compute the last components of the residual phase PS, i.e., the WFS aliasing and noise PS.

I. Wavefront-Sensor-Aliasing Power Spectrum

The phase aliasing error is defined in Eq. (16) as $\delta\varphi_{\mathrm{LF,HF}}=\overline{\mathcal{R}\{\mathcal{M}[\delta\varphi_{\mathrm{HF},a}]\}}$ where we recall that the overline represents the processes of both time lagging and time averaging during the WFS integration. Let us now compute its FT. We first note that the time lagging and averaging transform here is exactly as in the phase servo-lag FT, Eq. (30),

$$\widehat{\delta\varphi}_{\mathrm{LF,HF}}(\mathbf{f},t) = \sum_{n=1}^{N} \mathcal{F}\{\mathcal{R}\mathcal{M}[\delta\varphi_{\mathrm{HF},a}[h_n](\mathbf{r},t)]\} \times \mathrm{sinc}[\Delta t\mathbf{f}\cdot\mathbf{v}(h_n)]\exp[2\pi i t_l \mathbf{f}\cdot\mathbf{v}(h_n)], \tag{40}$$

and is not affected by the aliasing, which makes sense: WFS aliasing is a geometrical process and does not affect the dynamical properties of the phaselike time averaging/shifting. Let us now develop the FT term within Eq. (40). With Eq. (36) and Eq. (39), it becomes

$$\mathcal{F}\{\mathcal{R}\mathcal{M}[\delta\varphi_{\mathrm{HF},a}[h_n]]\} = [2\pi i f^2\,\mathrm{sinc}(\Lambda f_x)\mathrm{sinc}(\Lambda f_y)]^{-1}(\Lambda^2\{[f_x\widehat{\delta\varphi}_{\mathrm{HF},a}\,\mathrm{sinc}(\Lambda f_x)\mathrm{sinc}(\Lambda f_y)] * \mathrm{III}(\Lambda\mathbf{f})\}f_x + \Lambda^2\{[f_y\widehat{\delta\varphi}_{\mathrm{HF},a}\,\mathrm{sinc}(\Lambda f_x)\mathrm{sinc}(\Lambda f_y)] * \mathrm{III}(\Lambda\mathbf{f})\}f_y). \tag{41}$$

The next step is to replace the comb function by its Dirac distribution development,

$$\mathrm{III}(\Lambda\mathbf{f}) = \frac{1}{\Lambda^2}\sum_{k,l=-\infty}^{+\infty}\delta\left(f_x - \frac{k}{\Lambda}, f_y - \frac{l}{\Lambda}\right) \tag{42}$$

and with the equality

$$\frac{\mathrm{sinc}[\Lambda f_{(x,y)} - (k,l)]}{\mathrm{sinc}(\Lambda f_{(x,y)})} = \frac{(-1)^{(k,l)}\Lambda f_{(x,y)}}{\Lambda f_{(x,y)} - (k,l)}, \tag{43}$$

whence we finally find for the aliasing amplitude spectrum

$$\widehat{\delta\varphi}_{\mathrm{LF,HF}}(\mathbf{f},t) = \mu_{\mathrm{LF}}(\mathbf{f})\frac{f_x f_y}{f^2}\sum_{n=1}^{\mathrm{N}}\left\{\mathrm{sinc}[\Delta t\mathbf{f}\cdot\mathbf{v}(h_n)]\exp[2\pi i t_l \mathbf{f}\cdot\mathbf{v}(h_n)]\right.$$
$$\times\sum_{\substack{k,l=-\infty\\ |k|+|l|>0}}^{+\infty}\left[(-1)^{k+1}\left(\frac{f_x}{f_y-l/\Lambda}+\frac{f_y}{f_x-k/\Lambda}\right)\right.$$
$$\left.\left.\times\widehat{\delta\varphi}_{\mathrm{HF},a}[h_n]\left(f_x-\frac{k}{\Lambda},f_y-\frac{l}{\Lambda},t\right)\right]\right\}, \tag{44}$$

where the sum over the indices (k,l) is practically limited to a range of a few units in the implementation of the actual calculation, and the case $(k,l)=(0,0)$ is skipped, as the HF phase spectrum is null in the low-spatial-frequency range. Now, we can compute the aliasing PS. Assuming that the temporal correlation of the phase spectrum from $\mathbf{f}$ to $\mathbf{f}-(k,l)/\Lambda$ is negligible—which is acceptable as we know that the turbulent-phase PS drops sharply at high spatial frequency—and assuming as usual independence of the turbulent layers, we find

$$\Xi(\delta\varphi_{\mathrm{LF,HF}})(\mathbf{f}) = \mu_{\mathrm{LF}}(\mathbf{f})\frac{f_x^2 f_y^2}{f^4}\sum_{n=1}^{\mathrm{N}}\left(\mathrm{sinc}^2[\Delta t\mathbf{f}\cdot\mathbf{v}(h_n)]\right.$$
$$\times\sum_{\substack{k,l=-\infty\\ |k|+|l|>\infty}}^{+\infty}\left\{\left(\frac{f_x}{f_y-l/\Lambda}+\frac{f_y}{f_x-k/\Lambda}\right)^2 F_p\left(f_x-\frac{k}{\Lambda},f_y-\frac{l}{\Lambda}\right)\right.$$
$$\left.\left.\times{}^{\mathrm{M}}\Xi\{\delta\varphi_a[h_n]\}\left(f_x-\frac{k}{\Lambda},f_y-\frac{1}{\Lambda}\right)\right\}\right), \tag{45}$$

where the turbulent phase PS is piston-filtered, as usual. Equation (45) has singularities at $(f_x=0,k=0)$, $(f_y=0,l=0)$, and $(f_x,f_y)=(0,0)$. Calculation of the limits gives

$$\Xi\{\delta\varphi_{\mathrm{LF,HF}}\}(0,f_y) = \mu_{\mathrm{LF}}(0,f_y)\sum_{n=1}^{\mathrm{N}}\left\{\mathrm{sinc}^2[\Delta t f_y v_y(h_n)]\right.$$
$$\left.\times\sum_{\substack{l=-\infty\\ l\neq 0}}^{+\infty}F_p\left(0,f_y-\frac{l}{\Lambda}\right){}^{\mathrm{M}}\Xi\{\delta\varphi_a[h_n]\}\left(0,f_y-\frac{l}{\Lambda}\right)\right\}, \tag{46}$$

$$\Xi\{\delta\varphi_{\mathrm{LF,HF}}\}(f_x,0) = \mu_{\mathrm{LF}}(f_x,0)\sum_{n=1}^{\mathrm{N}}\left\{\mathrm{sinc}^2[\Delta t f_x v_x(h_n)]\right.$$
$$\left.\times\sum_{\substack{k=-\infty\\ k\neq 0}}^{+\infty}F_p\left(f_x-\frac{k}{\Lambda},0\right){}^{\mathrm{M}}\Xi\{\delta\varphi_a[h_n]\}\left(f_x-\frac{k}{\Lambda},0\right)\right\}, \tag{47}$$

$$\Xi(\delta\varphi_{\mathrm{LF,HF}})(0,0) = \mu_{\mathrm{LF}}(0,0)\sum_{n=1}^{\mathrm{N}}\sum_{\substack{k=-\infty\\ k\neq 0}}^{+\infty}F_p\left(-\frac{k}{\Lambda},0\right){}^{\mathrm{M}}\Xi\{\delta\varphi_a[h_n]\}\left(-\frac{k}{\Lambda},0\right),$$
$$= \mu_{\mathrm{LF}}(0,0)\sum_{n=1}^{\mathrm{N}}\sum_{\substack{l=-\infty\\ l\neq 0}}^{+\infty}F_p\left(0,-\frac{l}{\Lambda}\right){}^{\mathrm{M}}\Xi\{\delta\varphi_a[h_n]\}\left(0,-\frac{l}{\Lambda}\right). \tag{48}$$

J. Phase-Noise Power Spectrum

The WFS noise—in open loop—is a random quantity, with a white spectrum bounded to the LF domain $|f_x|,|f_y|<f_{\mathrm{WFS}}$. It is also discrete, defined only at the WFS sampling positions (centers of lenslets), and has the same unit as the WFS output, a two-component slope $\mathbf{n}_s(\mathbf{r},t)=[n_{s,x}(\mathbf{r},t),n_{s,y}(\mathbf{r},t)]$ for a SH-WFS.

The noise variance σ_n^2 is basically a function of the WFS integration time, guide star brightness and color, subaperture size relative to the telescope diameter, and a few other parameters that depend on the sophistication level of the WFS modeling and type (see Refs. 25 and 26 for WFS noise variance models).

From the WFS noise, the reconstructor gives rise to the phase noise term $\delta\varphi_{\mathrm{LF},n}$; see Eq. (16). Its amplitude spectrum is given by

$$\widehat{\delta\varphi}_{\mathrm{LF},n}(\mathbf{f},t)=\hat{\mathcal{R}}\cdot\hat{\mathbf{n}}_s(\mathbf{f},t)=\frac{f_x\hat{n}_{s,x}(\mathbf{f},t)+f_y\hat{n}_{s,y}(\mathbf{f},t)}{2\pi i f^2\,\mathrm{sinc}(\Lambda f_x)\mathrm{sinc}(\Lambda f_y)}, \tag{49}$$

from which it is straightforward to get the phase noise PS

$$\Xi\{\delta\varphi_{\mathrm{LF},n}\}(\mathbf{f})=\frac{\mu_{\mathrm{LF}}(\mathbf{f})N(\mathbf{f})}{4\pi^2 f^2\,\mathrm{sinc}^2(\Lambda f_x)\mathrm{sinc}^2(\Lambda f_y)}, \tag{50}$$

where we have assumed that the slope noise in x and y are not correlated and are of the same magnitude. $N(\mathbf{f})$ represents the spatial PS of the slope white noise, and is the same for both components of $\mathbf{n}_s$. It is constant within the domain $|f_x|,|f_y|<f_{\mathrm{WFS}}$ and zero outside, and is related to the noise variance by

$$\sigma_n^2=\int\int_{|f_x|,|f_y|<f_{\mathrm{WFS}}}N(\mathbf{f})\mathrm{d}^2 f=N\Lambda^2. \tag{51}$$

With this last equation, the presentation of the foundations of the phase-spatial PS method for analytical modeling of the adaptive-optics-point-spread function (AO-PSF) is terminated.

5. PAOLA

Our analytical method has been implemented in an IDL-based code, PAOLA, Performance of Adaptive Optics for Large or Little Apertures. Here, we present a few examples of execution on a Gemini-like telescope with a typical Mauna Kea turbulence profile. Atmosphere, telescope, and AO system parameters are given in Table 1. Most of the AO parameters correspond to the Gemini-

North AO system, ALTAIR (ALTitude-conjugate Adaptive optics for the InfraRed).

Figure 1 shows the aniso–servo PS [see Eq. (33)]. The symmetry of the PS is oriented toward the direction of the NGS, here +60°. The servo-lag error smooths out the anisoplanatism effect in the main wind direction, which was set here to +45°. In Fig. 2, we show the WFS aliasing PS [see Eqs. (45)–(48)]. Note that aliasing can be eliminated by low-pass filtering of the phase at the WFS input focal plane (see Ref. 28). The WFS noise PS is shown in Fig. 3 [see Eq. (50)]. Only the low spatial frequencies are affected by WFS noise. In Fig. 4 we show the total PS, the sum of the LF components plus the fitting error PS [see Eq. (22)]. A section of the phase PS before and after AO correction is shown in Fig. 5.

From the total LF and HF PS, we computed the LF and HF structure functions [Eq. (8)], Fig. 6. We see that both structure functions saturate at twice the phase variance (dashed–dotted lines), a fact that can be demonstrated by taking the infinite limit of Eq. (8). The structure functions oscillate with a period of ≈1.2 m, twice the DM actuator pitch (0.6 m). Such an oscillation is due to the sharp transition from the LF to HF domain in the DM spatial filter model, and we can expect in a real system this transition to be smoother, the oscillations less pronounced. The AO OTF calculated from the sum of the structure functions is shown in Fig. 7, after multiplication with the telescope OTF. Seeing-limited and telescope OTFs are shown for comparison. Figure 8 shows the associated PSF profiles. Within the corrected field half-width $\boldsymbol{\rho}_{ao}=\lambda f_{\mathrm{AO}}$ (here 0.287″) associated with the AO cutoff frequency, the AO PSF follows the telescope PSF, with an attenuation factor given by the Strehl ratio; as one gets closer to the $\boldsymbol{\rho}_{ao}$ boundary, the effect of aliasing can be seen as an increase of the PSF intensity; beyond, the PSF halo follows the seeing-limited PSF trend, with a few residual oscillations from the telescope PSF Airy rings. This interpretation comes from the fact that (1) the amplitude PSF (focal plane phasor) can be interpreted as the angular spectrum of the pupil phasor, and a feature in the pupil plane at a spatial frequency $\mathbf{f}$ will appear at the position $\lambda\mathbf{f}$ in the focal plane, and (2) in the small phase perturbation regime, i.e., $|\delta\varphi| \ll 1$ rad, the wings of the intensity PSF can be shown to be proportional to the phase PS (see Refs. 4 and 27). As a consequence, we can interpret the PS in terms of structures in the PSF: For instance the WFS noise will mainly affect the core of the PSF, the aniso–servo error will affect symmetrically the regions close to the PSF core in the direction of the NGS and the main wind direction, and the aliasing will generate a transition from the PSF diffraction-limited core to the PSF seeing-limited halo at the $\boldsymbol{\rho}_{ao}$ boundary.

We show now in the following figures some examples of AO parameter trade-off studies for a classical AO system on a Gemini-like telescope. The whole calculation for all cases took a couple of minutes to complete. In Fig. 9, we show the effect of the WFS temporal sampling frequency on the Strehl ratio, for four NGS magnitudes, 10, 11, 12, and 13. If the sampling frequency is optimized for each magnitude (respectively, 400, 200, 130 and 100 Hz for the example AO system chosen here), then the Strehl ratio can be kept above 60%. On the left of the same figure, we note that the different magnitude cases overlap: This is explained by the fact that at low sampling frequency, i.e., long integration time, the noise spectrum is greatly reduced, leaving the servo-lag error as the main component of the phase error, which is independent of the NGS mag-

Table 1. Atmosphere, Telescope, and Adaptive Optics System Parameters

Telescope and Atmosphere		AO System	
∅ M1,2	7.9, 1.2 m	Actuator density	1
λ	1.65 μm	DM height	0 km
Seeing	0.7″	NGS angle	5″
$r_0(\lambda)$	0.605 m	NGS orientation	60°
L_0	30 m	WFS int. time	10 ms
$\langle H_{\mathrm{layers}}\rangle$	6636 m	Loop time lag	0.8 ms
$\theta_0(\lambda)$	5.9″	NGS magnitude	12
$\langle V_{\mathrm{layers}}\rangle$	19.3 m/s	NGS temperature	6000 K
$\tau_0(\lambda)$	9.8 ms	WFS readout noise	5 e/px

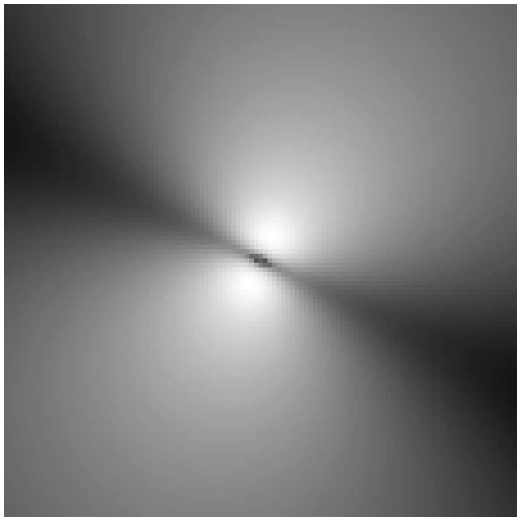

Fig. 1. Aniso–servo power spectrum (1/8 power-law scaling) within the LF domain; see parameters in Table 1.

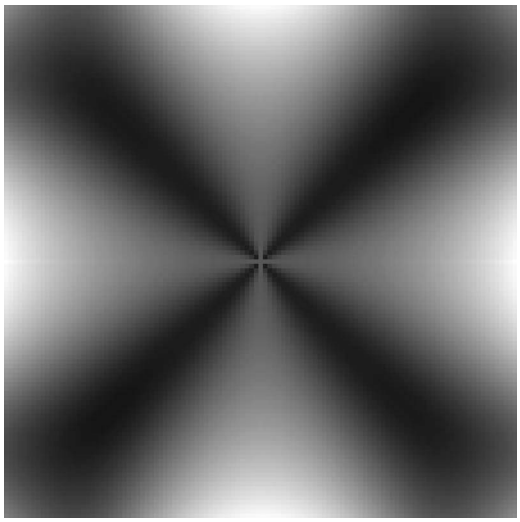

Fig. 2. Aliasing power spectrum (1/8 power-law scaling) within the LF domain; see parameters in Table 1.

nitude. At high sampling frequency, the inverse situation occurs, and curves for different magnitudes no longer overlap.

Figure 10 shows the effect of DM actuator density, defined as Λ/r_0, for the same NGS magnitudes as above. For low actuator density, HF phase and aliasing dominate the error, so curves overlap as before. At high actuator density, the spreading of the NGS photons into more and more subapertures decreases the WFS signal-to-noise ratio: The optimal actuator density is indeed a function of the NGS magnitude.

Finally, we show in Fig. 11 the effect of the anisoplanatism error on the 50% encircled energy diameter (EED) for a NGS off-axis separation of 0 to 30″, for our usual magnitudes. For an on-axis NGS, we see basically the effect of WFS noise, servo-lag, and aliasing. Increasing the off-axis NGS angle obviously increases the EED. Let us assume that for a significant improvement of

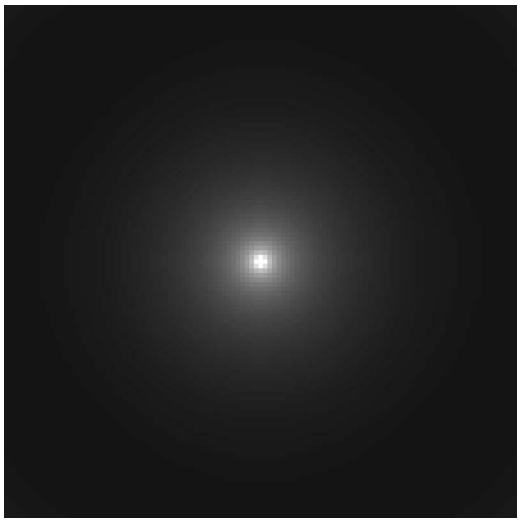

Fig. 3. WFS noise power spectrum (1/8 power-law scaling) within the LF domain; see parameters in Table 1.

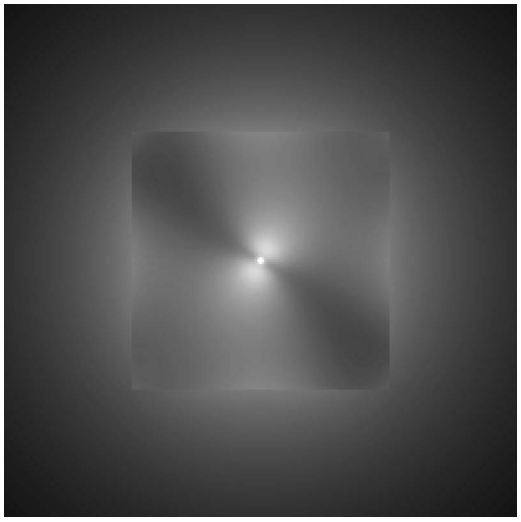

Fig. 4. Total phase power spectrum (1/8 power-law scaling). Spatial frequency domain has been extended to twice the LF boundary to show the fitting error power spectrum. Note the square boundary between the low (corrected) and the high spatial frequency domains. See parameters in Table 1.

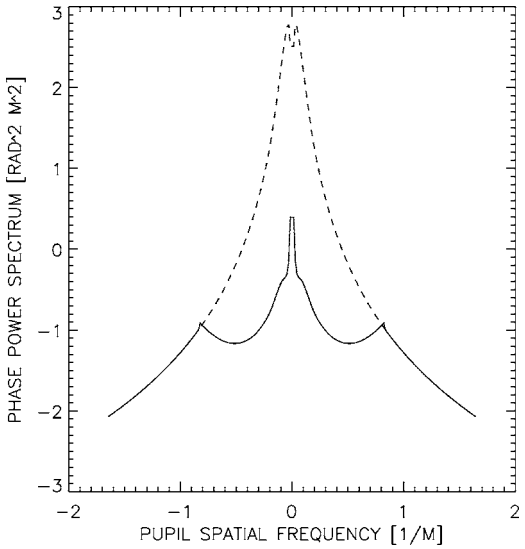

Fig. 5. f_x-cut across the total phase power spectrum shown in Fig. 4. Dashed curve shows the turbulent, uncorrected phase power spectrum.

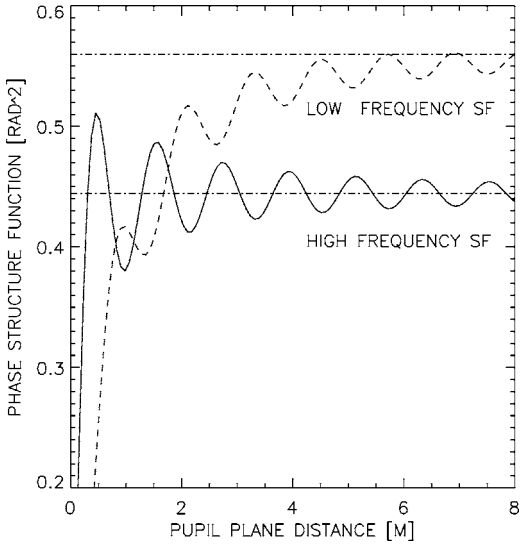

Fig. 6. Fitting error and LF phase structure functions. Horizontal dashed–dotted lines represent twice the fitting error and LF variances. See parameters in Table 1.

a spectroscopic measurement, the EED has to be reduced by a factor of two relative to the seeing-limited case. Then, the field of correction diameter will be ~16″ to 10″ for 10th to 12th magnitude NGS, and zero (no corrected field available) when using a 13th magnitude star. With such a result, and using star-count models, it is easy to evaluate what would be the sky coverage for this particular system and instrument.

In our opinion, a natural application of our code would be to serve as a PSF performance evaluation tool for a given system on a given telescope: The astronomer sets the parameters of the AO run (seeing and AO system), and PAOLA gives automatically and rapidly the expected PSF and OTF, allowing the observer to decide if it is worthwhile to run the observation, and if so, to have an

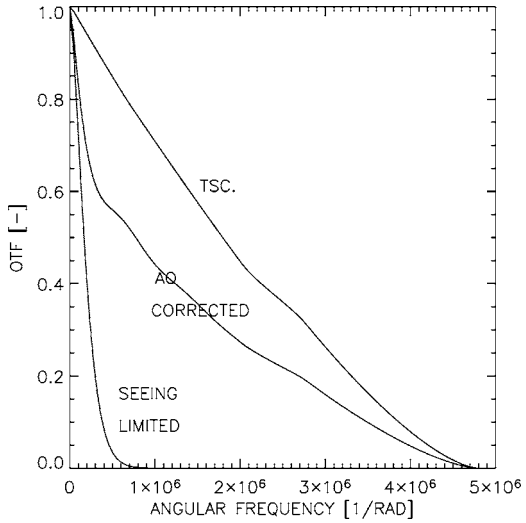

Fig. 7. Long exposure OTFs for the telescope, the telescope with an AO corrected phase (associated with the structure functions shown in the Fig. 6), and the telescope with an uncorrected turbulent phase. See parameters in Table 1.

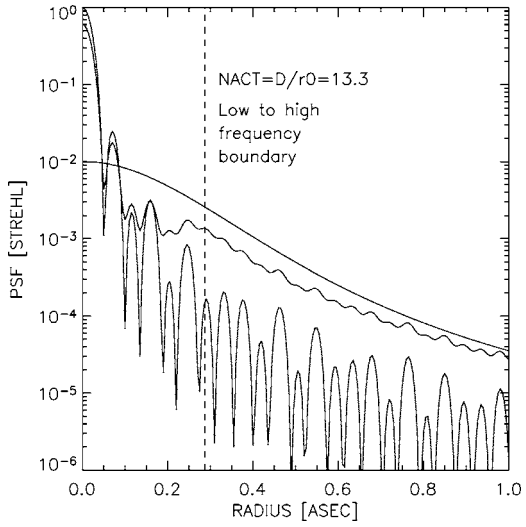

Fig. 8. Long exposure PSF profiles associated with the OTFs shown in Fig. 7.

evaluation of the associated PSF for *a posteriori* data processing.

As a last example, we show in Figs. 12 and 13 an extreme-contrast AO (ExAO), instantaneous PSF calculated with a MC E2E code and PAOLA, for comparison. In order to avoid WFS aliasing, spatial filtering of the HF phase error was implemented into the MC simulation (see Ref. 28). With PAOLA, spatial filtering of HF is simulated simply by not adding the WFS aliasing component to the total residual phase PS. The square field of AO correction below angular distance $\boldsymbol{\rho}_{ao}$ is apparent in both cases. This example illustrates an interesting application of our code: The residual PS can be calculated with PAOLA, and used to create AO-corrected phase screens for coronagraphy and speckle effects studies.

We wanted to show with these few examples how easy and fast it is to get a good estimate of the performance of a given AO system using the analytical method. Once the properties of the AO system have been understood, a complete, detailed MC E2E model can be built to get a more detailed analysis of the system's performance, including second-order effects not seen in the first-order analysis.

6. CONCLUSIONS

In this paper, we give the fundamental basis for the first-order analytical modeling of the long-exposure optical transfer function (OTF) of a telescope with adaptive optics (AO). The method relies on the relationship between the residual phase spatial power spectrum and structure function on one hand, and between the structure function and the long-exposure AO OTF on the other. This OTF is multiplied by the telescope OTF to get the total OTF. Once the OTF is obtained, getting the long-exposure point-spread function (PSF) is simply a matter of computing a numerical Fourier transform. Comparisons with Monte Carlo simulations show good agreement.

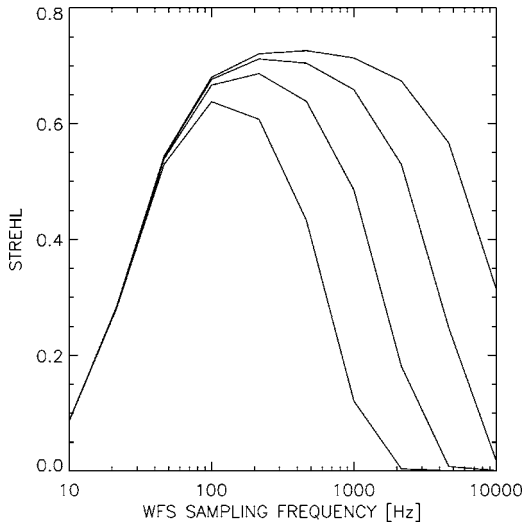

Fig. 9. Strehl ratio versus WFS sampling frequency. NGS magnitude from 10 (top curve) to 13 (bottom). See other parameters in Table 1.

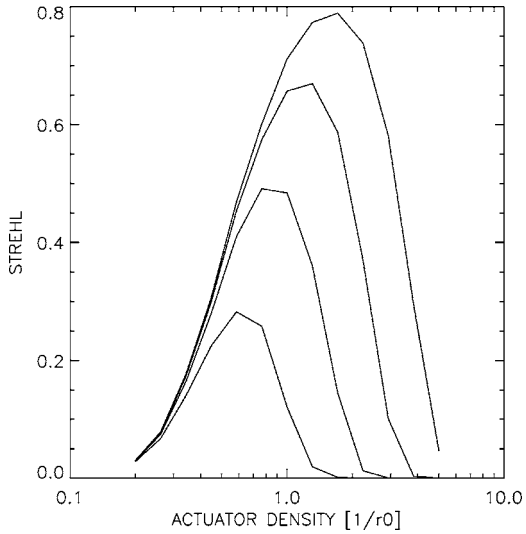

Fig. 10. Strehl ratio versus DM actuator density. NGS magnitudes from 10 (top curve) to 13 (bottom). See other parameters in Table 1.

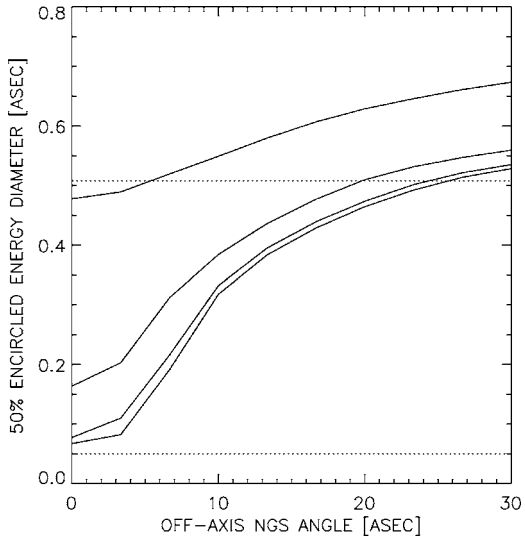

Fig. 11. 50% encircled energy diameter versus NGS off-axis angle. NGS magnitude from 10 (bottom curve) to 13. Horizontal dashed lines: top, seeing-limited case; bottom, diffraction-limited case.

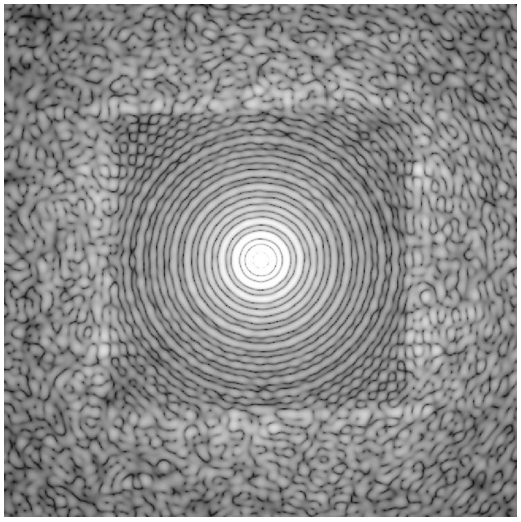

Fig. 12. Monte Carlo end-to-end extreme AO simulation: instantaneous PSF (log scale). Telescope diameter 7.9 m, wavelength 1.65 μm, 44 actuators across the DM, seeing 0.95″, outer scale 30 m, Strehl ratio 95%. WFS aliasing has been optically filtered (courtesy of B. Macintosh and L. Poyneer, poyneer@llnl.gov).

The model presented here is for a Shack–Hartmann wavefront sensor, with a least-square type reconstructor. Nevertheless, other wavefront sensor type modeling is possible in principle, as it has already been done for a pyramid sensor.[24] The next step would be to build a curvature-sensing model. Such models are useful in making quick comparisons of the performance of different wavefront sensor types regarding noise propagation and aliasing issues.

The deformable mirror model we have used here is a perfect spatial filter one. In practice, deformable mirror transfer functions are not so sharp, and in principle we should be able to make our model more realistic by using measured, empirical, deformable-mirror spatial transfer functions, instead of the perfect masks we have used here.

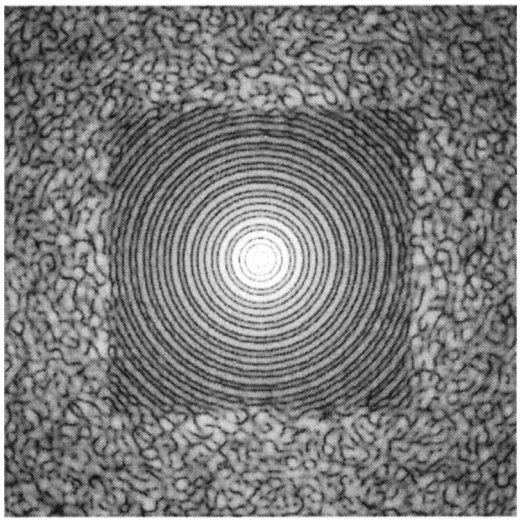

Fig. 13. PAOLA extreme AO simulation; same conditions as Fig. 12. The PSF has been calculated from an AO-corrected phase screen that was built using a phase power spectrum calculated with the code PAOLA (courtesy of R. Soummer, soummer @stsci.edu).

In summary, the theory presented here can be used as the basis on which to build more and more sophisticated analytical models, including new types of wavefront sensors, reconstructors, and deformable-mirror influence functions, as long as these models have a practical formulation in the pupil-plane spatial frequency domain.

ACKNOWLEDGMENTS

L. Jolissaint thanks the Fond National Suisse de la Recherche Scientifique for their financial support during this work. We thank also the members of the PAOLA user group for their suggestions for improving the code, and the reviewers for their very useful comments and suggestions. Corresponding author L. Jolissaint's e-mail address is laurent.jolissaint@nrc-cnrc.gc.ca.

REFERENCES

1. M. Le Louarn, "Parallel simulation tools for AO on ELTs," in Proc. SPIE **5490**, 705–712 (2004).
2. T. Fusco and J.-M. Conan, "On- and off-axis statistical behavior of adaptive-optics-corrected short-exposure Strehl ratio," J. Opt. Soc. Am. A **21**, 1277–1289 (2004).
3. F. Rigaut, J.-P. Véran, and O. Lai, "An analytic model for Shack–Hartmann based adaptive optics systems," in Proc. SPIE **3353**, 1038–1048 (1998).
4. L. Jolissaint and J.-P. Véran, "Fast computation and morphologic interpretation of the adaptive optics point spread function," in *Beyond Conventional Adaptive Optics*, E. Vernet, R. Ragazzoni, S. Esposito, and N. Hubin, eds., Vol. 58 of European Southern Observatory Conference and Workshop Proceedings, 201–208 (ESO, 2001).
5. A. Tokovinin, "Seeing improvement with ground-layer adaptive optics," Publ. Astron. Soc. Pac. **116**, 941–951 (2004).
6. L. Jolissaint, J.-P. Véran, and J. A. Stoesz, "Wide field adaptive optics upper limit performances," in Proc. SPIE **5382**, 468–477 (2004).
7. L. Jolissaint and J.-F. Lavigne, "An analytic model for the study of the impact of mirror segmentation on AO performance, and application to a 30 m segmented telescope," in Proc. SPIE **5497**, 1038–1048 (2004).

8. B. L. Ellerbroek, "Linear systems modeling of adaptive optics in the spatial-frequency domain," J. Opt. Soc. Am. A **22**, 300–322 (2005).
9. C. Aime and R. Soummer, "The usefulness and limits of coronagraphy in the presence of pinned speckles," Astrophys. J. **612**, L85–L88 (2004).
10. B. Gillespie, R. Carlberg, T. Davidge, J. J. Kavelaars, D. Crabtree, M. Hudson, B. Oke, C. Morbey, L. Abraham, L. Jolissaint, J.-P. Véran, K. Fulbright, P. Stetson, and D. Bohlender, "The science case and instrumentation for extra large telescopes," Report for the Extra Large Telescope Canadian Project, Tech. Rep. (Herzberg Institute of Astrophysics, National Research Council of Canada, 2001).
11. O. Lardiere, P. Salinari, L. Jolissaint, M. Carbillet, A. Riccardi, and S. Esposito, "Adaptive optics and site requirements for the search of earth-like planets with ELTs," in Proc. SPIE **5382**, 550–559 (2004).
12. J. A. Stoesz, D. Andersen, and L. Jolissaint, "GLAO feasibility study report for Gemini telescopes." Tech. Rep. GLAO-PRD-001 (Herzberg Institute of Astrophysics, National Research Council of Canada, 2005).
13. T. Travouillon, J. S. Lawrence, and L. Jolissaint, "Ground layer adaptive optics performance in Antarctica," in Proc. SPIE **5497**, 934–942 (2004).
14. Canadian VLOT [Very Large Optical Telescope] Working Group, *VLOT Project Book. A Large Optical Telescope for the 21th Century* (Herzberg Institute of Astrophysics, National Research Council of Canada, Victoria, British Columbia, Canada, 2003).
15. J.-M. Conan, *Etude de la Correction Partielle en Optique Adaptative* (Office National d'Etude et de Recherche Aérospatiale, Paris, 1995).
16. J.-P. Véran, F. Rigaut, H. Maître, and D. Rouan, "Estimation of the adaptive optics long-exposure point spread function using control loop data," J. Opt. Soc. Am. A **14**, 2957–3069 (1997).
17. F. Roddier, "The effect of atmospheric turbulence in optical astronomy," in *Progress in Optics, Vol. XIX*, E. Wolf, ed. (North-Holland, 1981), pp. 281–376.
18. V. I. Tatarski, *Wave Propagation in a Turbulent Medium*, (Dover, 1961), translated by R. A. Silverman.
19. D. L. Fried, "Optical resolution through a randomly inhomogeneous medium for very long and very short exposures," J. Opt. Soc. Am. **56**, 1372–1379 (1966).
20. E. Weisstein, "Jensen's Inequality," http://mathworld.wolfram.com/JensensInequality.html.
21. J.-P. Véran, "Estimation de la réponse impulsionelle et restauration d'image en optique adaptative," Ph.D. thesis (Ecole Nationale Supérieure des Télécommunications, Paris, 1997).
22. C. Innocenti and A. Consortini, "Estimate of characteristics scales of atmospheric turbulence by thin beams: comparison between the von Karman and Hill–Andrews models," J. Mod. Opt. **51**, 333–342 (2004).
23. R. J. Sasiela, "Wave-front correction by one or more synthetic beacons," J. Opt. Soc. Am. A **11**, 389–393 (1994).
24. C. Verinaud, "On the nature of the measurements provided by a pyramid wave-front sensor," Opt. Commun. 233, (2004).
25. G. Rousset, "Wavefront sensing," in *NATO ASIC Proc. 423: Adaptive Optics for Astronomy* (1994), p. 115.
26. B. L. Ellerbroek and R. A. Buchroeder, "Near-infrared AO coronagraph design for giant telescopes," in Proc. SPIE **4840**, 404–411 (2003).
27. A. Sivaramakrishnan, P. E. Hodge, R. B. Makidon, M. D. Perrin, J. P. Lloyd, E. E. Bloemhof, and B. R. Oppenheimer, "The adaptive optics point-spread function at moderate and high Strehl ratios," in Proc. SPIE **4860**, 161–176 (2003).
28. L. A. Poyneer and B. Macintosh, "Spatially filtered wave-front sensor for high-order adaptive optics," J. Opt. Soc. Am. A **21**, 810–819 (2004).